nature geoscience

Article

https://doi.org/10.1038/s41561-024-01574-3

Cryptic degassing and protracted greenhouse climates after flood basalt events

Received: 3 June 2023

Accepted: 24 September 2024

Published online: 30 October 2024

Check for updates

Benjamin A. Black[1] ✉, Leif Karlstrom[2], Benjamin J. W. Mills[3], Tamsin A. Mather[4], Maxwell L. Rudolph[5], Jack Longman[6] & Andrew Merdith[7]

Large igneous provinces erupt highly reactive, predominantly basaltic lavas onto Earth's surface, which should boost the weathering flux leading to long-term CO_2 drawdown and cooling following cessation of volcanism. However, throughout Earth's geological history, the aftermaths of multiple Phanerozoic large igneous provinces are marked by unexpectedly protracted climatic warming and delayed biotic recovery lasting millions of years beyond the most voluminous phases of extrusive volcanism. Here we conduct geodynamic modelling of mantle melting and thermomechanical modelling of magma transport to show that rheologic feedbacks in the crust can throttle eruption rates despite continued melt generation and CO_2 supply. Our results demonstrate how the mantle-derived flux of CO_2 to the atmosphere during large igneous provinces can decouple from rates of surface volcanism, representing an important flux driving long-term climate. Climate–biogeochemical modelling spanning intervals with temporally calibrated palaeoclimate data further shows how accounting for this non-eruptive cryptic CO_2 can help reconcile the life cycle of large igneous provinces with climate disruption and recovery during the Permian–Triassic, Mid-Miocene and other critical moments in Earth's climate history. These findings underscore the key role that outgassing from intrusive magmas plays in modulating our planet's surface environment.

Large igneous provinces (LIPs) have been linked with major disruptions of Earth systems, including four of the five major mass extinctions of the Phanerozoic[1–3]. LIP volcanism and metamorphic degassing driven by shallow intrusions[4] are often considered as a driver of transient spikes in atmospheric CO_2 such as the Palaeocene–Eocene Thermal Maximum (PETM)[5] and the end-Permian mass extinction[6,7]. However, the manner in which waning LIP activity has shaped climate recovery from such catastrophic disruptions has received less attention.

LIPs with high-resolution geochronology and palaeoclimate proxy records—tracking the tempo of volcanism and environmental changes, respectively—include the Columbia River Basalts (CRB), North Atlantic Igneous Province (NAIP), Deccan Traps and Siberian Traps. For each of these LIPs, we identify a pattern of protracted warming spanning several Myr after voluminous flood basalt eruptions (Fig. 1). For example, following the end-Permian mass extinction 252 million years ago (Ma), hothouse conditions, elevated CO_2 and continued carbon cycle

[1]Department of Earth and Planetary Sciences, Rutgers University, Piscataway, NJ, USA. [2]Department of Earth Sciences, University of Oregon, Eugene, OR, USA. [3]School of Earth and Environment, University of Leeds, Leeds, UK. [4]Department of Earth Sciences, University of Oxford, Oxford, UK. [5]Department of Earth and Planetary Sciences, University of California-Davis, Davis, CA, USA. [6]Department of Geography and Environmental Science, Northumbria University, Newcastle Upon Tyne, UK. [7]School of Physics, Chemistry and Earth Sciences, University of Adelaide, Adelaide, Australia. ✉e-mail: bblack@eps.rutgers.edu

https://doi.org/10.1038/s41561-024-01574-3

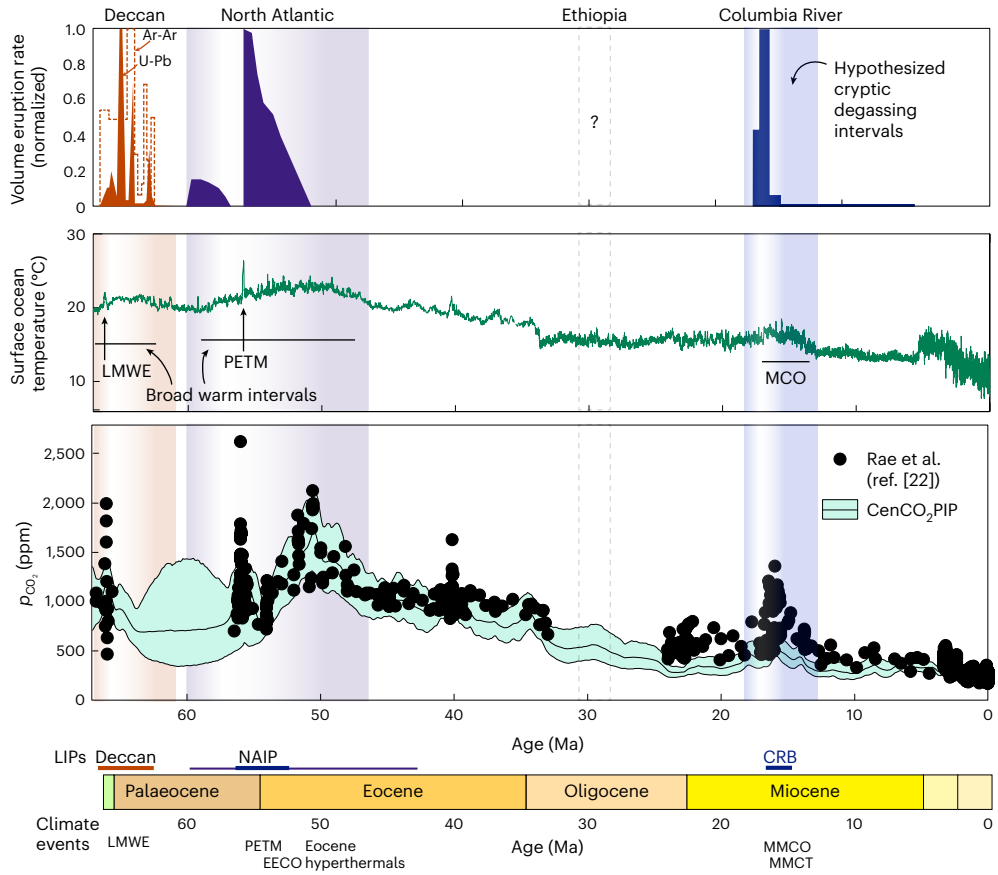

Fig. 1 | Records of Cenozoic LIP volcanism, climate and atmospheric CO_2. Delayed recovery from greenhouse climates (LMWE, Latest Maastrichtian Warming Event; PETM, Palaeocene–Eocene Thermal Maximum; MCO, Miocene Climatic Optimum; shown as shaded bands) associated with Cenozoic LIPs lasts well beyond the end of LIP main phase volcanism[12,54–56] (top panel). Cenozoic surface temperature variations are from the CENOGRID compilation of marine oxygen isotope records[22], with CO_2 from boron isotopes[23] and the CenCO2PIP multi-proxy intercomparison project[26] (blue shading is 95% confidence interval). pCO_2, atmospheric CO_2 partial pressure.

perturbations persisted for ~5 Myr (refs. 8–10), ~3 Myr beyond the age of the youngest known Siberian Traps volcanic rocks[11]. Most recently, the warmest temperatures of the Mid-Miocene Climatic Optimum (MMCO) from 16–14 million years ago postdated the main phase of CRB volcanism by 1–2 Myr (ref. 12) (Fig. 1). These observations have motivated a hypothesis that the silicate weathering feedback—thought to be the fundamental thermostat regulating our planet's climate[13]—breaks down or is weakened during these events[10,14]. However, the contribution of intrusive LIP carbon emissions, independent of surface lava extrusion, to variations in atmospheric CO_2 and global surface temperatures on long (10^6 year) timescales has not been studied in detail. Here we test the hypothesis that observed delays in recovery reflect prolonged CO_2 degassing from lithospheric LIP magma plumbing systems, without necessarily altering the silicate weathering thermostat. Specifically, we propose that cryptic CO_2 release from intrusive magmas—also known as diffuse or non-eruptive outgassing—continues from deeper portions of LIP magmatic systems long after surface volcanism wanes (Fig. 2) and that for some—but not necessarily all—LIPs, these emissions prolong climatic warming.

High-precision geochronology now constrains the 'main phase' of volcanism and shallow intrusive activity in many continental LIPs to <1 Myr (ref. 15). However, main phase extrusive rocks and upper crustal sills represent a minor fraction of the total volume of mantle melt expected from geodynamic modelling, seismic surveys and petrologic estimates of the intrusive to extrusive (*I*:*E*) ratio[16–18]. This disparity is expected: for continental LIPs, the crust acts as a time-evolving thermomechanical filter for the ascent and eruption of mantle-derived melts[18–20]. Seismic data support the presence of large volumes of LIP intrusions at Moho to middle crustal depths[16,17], perhaps associated with neutral buoyancy[16–18].

Here we argue that thermally controlled rheologic transitions in the crust can in some cases create a stabilizing feedback that inhibits magma ascent, shutting off extrusive volcanism. Such a thermomechanical throttle on magma ascent provides a mechanism to decouple CO_2 release from volcanic eruption rates, assuming fluids rich in CO_2 from deep intrusive magmas can transit the crust even when magmas are not erupting. Consequently, cryptic CO_2 release may continue for the duration of mantle melting as vapour-saturated intrusions cool, crystallize and exsolve CO_2. Analogous cryptic CO_2 outgassing has been inferred for the present-day East African Rift[20,21], demonstrating the potential occurrence of this process and the likelihood that the majority (or at least substantial proportions) of CO_2 in even deep intrusive magmas exsolves and reaches the atmosphere. Here we consider the hypothesis that this mechanism explains protracted high CO_2 and warm climate during the early Triassic and MMCO but also during other events such as the Early Eocene Climatic Optimum (EECO; ~53–49 Ma, here linked with the waning phases of NAIP) that have not traditionally been connected with LIPs because they postdate the most voluminous surface volcanism.

Protracted warmth at odds with the tempo of volcanism

To test this hypothesis, we examine high-resolution climate and atmospheric CO_2 records[22–26] where they exist, spanning events including

https://doi.org/10.1038/s41561-024-01574-3

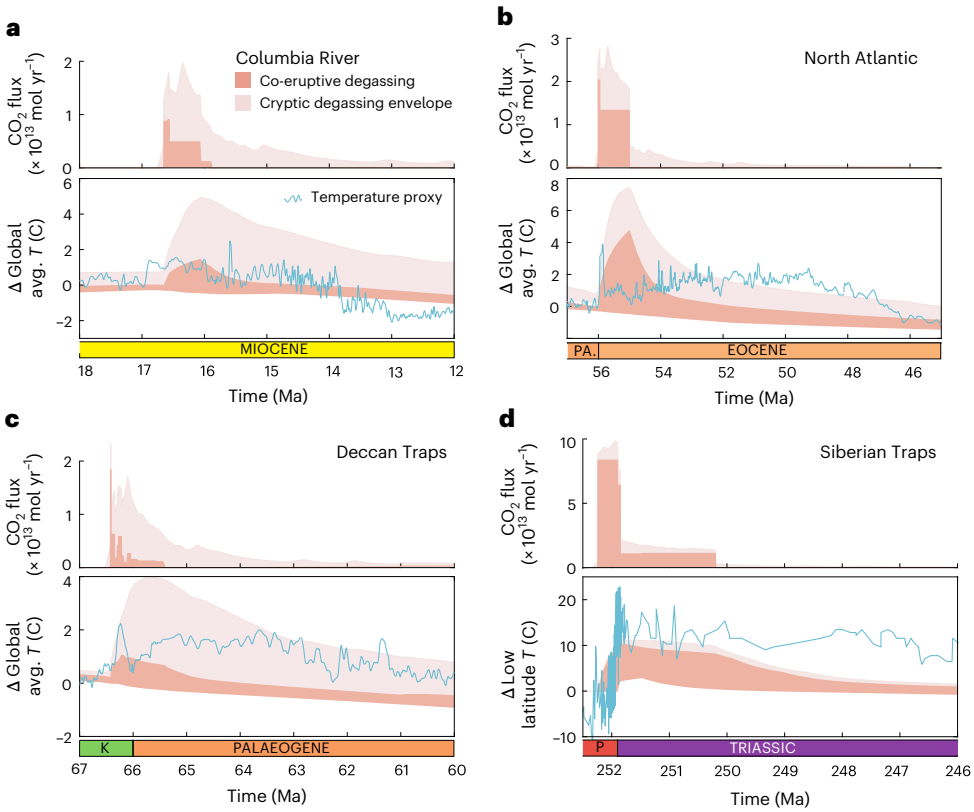

Fig. 2 | Cryptic degassing provides a missing carbon flux needed to reconcile model predictions with climate records. a–**d**, Comparison of observed climate histories[22,24,25] with SCION model predictions for Columbia River Basalts (**a**), North Atlantic Igneous Province (**b**), Deccan Traps (**c**) and Siberian Traps (**d**). Co-eruptive degassing scenarios account for erupted lavas, co-eruptive CO_2 release from intrusions and metamorphic CO_2 estimates for the Siberian Traps and NAIP (dark shading reflects a range in assumed magmatic CO_2 and a range in intrusive to extrusive ratios from 1:1 to 10:1; Methods). Combinations of volcanic, intrusive and metamorphic carbon synchronized with eruptive tempo are insufficient to explain the observed protracted warming. Light shaded envelope represents the range of climate responses for the range of cryptic degassing expected based on mantle plume melting models (Methods and Supplementary Fig. 2). PA, Paleocene; K, Cretaceous; P, Permian.

the CRB, NAIP and Deccan and Siberian Traps (Figs. 1 and 2). We identify a dual tempo of climate response to LIP CO_2 outgassing covering the periods recorded by these datasets comprising both brief, rapid warming (spanning 10^4–10^5 years) and several-million-year-long more stable warm intervals (Fig. 1). Rapid warming episodes include the PETM, the ~66.3 Ma Late Maastrichtian Warming Event and the end-Permian mass extinction. Sulfate aerosols may drive cooling on 10^1–10^2-year timescales[27], but this is unlikely to be resolved in palaeoclimate records[6]. Broad periods of warm climate and high CO_2 include the early Triassic, the MMCO, subtle warming in the earliest Palaeocene and the EECO.

Brief, geologically rapid warming has been widely attributed to a combination of volcanism, shallow intrusive activity and thermal metamorphism[5,7,28]. In contrast, the protracted warm periods captured by these records have typically not been linked with LIPs because the warming lags volcanism[29]. Proposed explanations for these warmhouse and hothouse intervals include variations in mid-ocean ridge CO_2 outgassing[30] and elevated sediment subduction during closure of Tethys[31]. However, the net effects of mid-ocean ridge outgassing on atmospheric pCO_2 are unclear[32,33], and Tethyan subduction CO_2 fluxes are insufficient to explain Eocene warmth[34]. To test whether CO_2 release from a combination of extrusive and metamorphic sources can adequately explain the full temperature histories including broad multi-million-year warming intervals, we reconstruct outgassing for the Siberian Traps, Deccan Traps, NAIP and CRB based on eruption histories (Supplementary Table 1). Each of these outgassing scenarios incorporates uncertainties in initial magma CO_2 concentrations. In the case of the Siberian Traps and NAIP, we further include scenarios that account for outgassing from metamorphism of hydrocarbons and sedimentary rocks in the Tunguska and North Atlantic basins, respectively[5,35].

Climate–biogeochemical modelling with the SCION model (Methods), which includes CO_2 drawdown enhanced by newly emplaced basalts, demonstrates that volcanic outgassing histories alone cannot explain observations based on climate proxy records (Fig. 2). Scenarios that combine intrusive, volcanic and metamorphic CO_2 release can reconcile LIP emissions with the magnitude of warming during some brief warming episodes associated with the onset and main phase of volcanism[4,36,37]. However, the observed tempo of climate recovery following CRB, Deccan Traps and Siberian Traps volcanism is still much slower than predicted by climate–biogeochemical modelling even when scenarios accounting for metamorphic degassing and intrusive contributions are added to eruptive CO_2 budgets (Fig. 2)—if we assume that intrusive degassing occurs at the same time as surface eruptions. Maintaining the observed long-term surface warming therefore requires either a transient breakdown in the fundamental silicate weathering feedback, carbon release beyond the youngest dated rocks in the main volcanic sequences or other currently unknown processes. Such shifts in the weathering feedback have been proposed for the early Triassic in particular[29,38], possibly driven by carbon cycle restructuring during the end-Permian mass extinction. However, extended warming also follows LIPs that are not related to mass extinctions, such as the NAIP and CRB.

https://doi.org/10.1038/s41561-024-01574-3

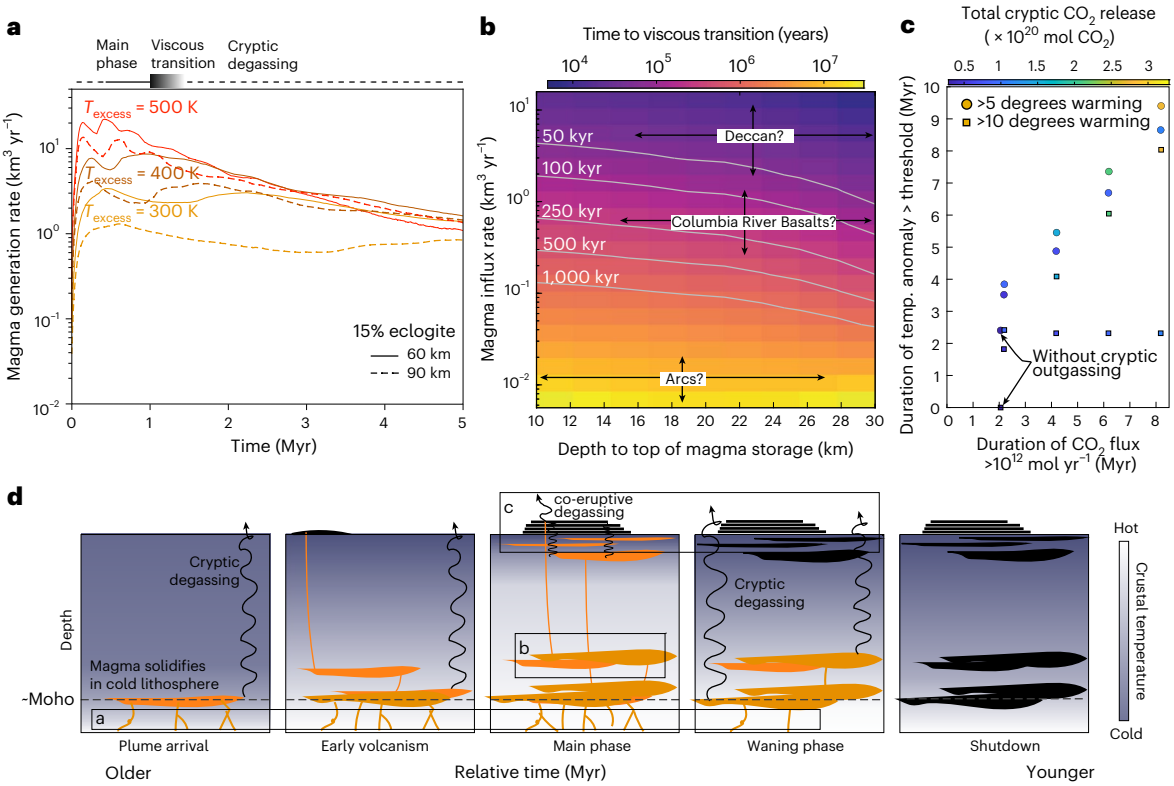

Fig. 3 | Geodynamic and thermomechanical calculations guide expectations for the evolution of LIPs. a, Mantle melting is predicted to last 5 Myr or more. **b**, A rheological transition in the crust on timescales of ~10^5 years throttles ascent of magmas from deeper storage regions. **c**, SCION sensitivity tests for the end-Permian with median Siberian Traps co-eruptive outgassing and cryptic degassing ranging from 10^{13} to 3×10^{13} mol CO_2 yr^{-1} for 2, 4, 6 or 8 Myr, showing that maintaining a given level of warming requires a minimum CO_2 flux; if cryptic degassing satisfies this flux, the duration of warming depends on the duration of cryptic degassing and cumulative emissions. **d**, The combined influence of prolonged mantle melting and declining surface volcanism decouples CO_2 flux from volcanic output, with high cryptic CO_2 fluxes during early and waning phases of LIP emplacement. During early emplacement, magmas solidify in the cold lithosphere, exsolving gas. During late emplacement, the rheologic shift shown in **b** inhibits eruptions, but cryptic degassing continues from magmas solidifying in the lower crust and mantle lithosphere.

Waning surface eruptions despite long-lived mantle melting

To test whether carbon release beyond the youngest preserved/dated LIP rocks is plausible, we have modelled the time evolution of both melt generation and crustal transit of magmas relevant for continental LIPs. Our geodynamic simulations of LIP melt generation by mantle plume head decompression melting (Methods) demonstrate that voluminous (10^6–10^7 km^3; Fig. 3a and Supplementary Fig. 1) LIP melting should last ~5 Myr or more during initial plume impingement[18,39,40]. This long duration of melt production contrasts with <1 Myr main phase volcanic activity for many LIPs[41]. Peak melt production rates for the highest excess temperature scenario are 20–30 km^3 yr^{-1}, around one order of magnitude larger than time-averaged main phase LIP eruption rates[42] and two orders of magnitude larger than melt supply estimates at Hawaii.

Thermomechanical modelling of crustal evolution associated with magma ascent and storage (Methods) demonstrates how feedbacks in material properties create a crustal rheological throttle capable of decoupling eruptions from mantle supply. During main phase volcanism, magmas heat the crust during transit and can induce viscous relaxation over the depth-range where intrusions occur on ~10^5-year timescales (Fig. 3b), enabling stresses to dissipate more rapidly than they build up. This inhibits magma reservoir failure and magma ascent[41,3]. A transition to dominantly ductile (versus elastic) crustal rheology then curtails eruptions at the surface despite abundant plume-fed melt present at depth, instead promoting crustal magma storage. Our modelling shows that this transition occurs on timescales comparable to the main phase of flood basalt volcanism in the CRB, Deccan Traps and Siberian Traps (Fig. 3b). The progression and efficacy of crustal throttling depend on storage depth, crustal rheology, background tectonic motions and magma influx, with the interplay between these factors plausibly reflected in the variable duration and tempo of main phase volcanism for different LIPs.

Considered together, protracted timescales of mantle melting and rheological decoupling of surface volcanic fluxes from the supply of volatile-rich magma to the lithosphere support the hypothesis that crystallization of deep, vapour-saturated LIP magmatic systems can drive cryptic CO_2 degassing even if there is no surface volcanic expression (Fig. 3c). Volumetrically subordinate alkaline and silicic volcanism characterize the waning stage of many continental LIPs, providing further evidence for long-lived supply of magma and heat to the lithosphere.

The transfer of exsolved CO_2 from deep intrusive bodies to the atmosphere depends on crustal permeability. Hydrofracturing associated with dike and sill emplacement during the main phase of LIP volcanism is expected to create extensive damage zones consistent with relatively high deep permeability (10^{-16}–10^{-19} m^2) observed in modern active magmatic settings[43,44]. The flux of CO_2 and other exsolved volatiles from intrusions in the shallow, brittle crust is thus expected to be efficient. However, direct measurements of permeability are limited to the uppermost few km of the crust, and much remains unknown about transfer of fluids from the ductile lower crust[45]. Beneath the brittle–ductile transition, ductile deformation will act to heal damage and reduce permeability. Work on metamorphic systems suggests expulsion of CO_2 from the lower crust is still possible in response to

build-up of pore pressure but may come in pulses known as porosity waves[46] rather than a steady trickle. Studying present-day patterns and fluxes of cryptic degassing is challenging given their wide spatial scale, however, degassing scenarios based on measurements in the East African Rift suggest potential CO_2 release from lower crustal or even mantle lithospheric depths via fault systems[20,21].

We conduct an ensemble of mantle geodynamic simulations that encompass uncertainties in key parameters including mantle potential temperature and CO_2 concentrations in peridotitic and eclogitic mantle (Methods) to calculate envelopes for CO_2 available for cryptic degassing. Assuming a mantle plume comprising 5–25% eclogite and the remainder peridotite with 900–1,800 and 137–400 ppm CO_2, respectively (Methods), these simulations predict mobilization of ~10^{12}–10^{13} mol CO_2 yr^{-1} from the mantle for several million years beyond the timeline of main phase volcanism (Supplementary Fig. 1). These geodynamically modelled mantle CO_2 extraction rates are in good first-order agreement with the continued degassing required to explain observed warming during the MMCO, EECO and Palaeocene (Fig. 2) based on climate–biogeochemical simulations with SCION (Methods). In the case of the early Triassic, cryptic degassing extends warming, but observed warming lasts even beyond the cryptic degassing scenario shown here. Sensitivity tests with SCION for the end-Permian (Fig. 3c) show that once a critical CO_2 flux for a given warming threshold is satisfied, the timescales of protracted warming directly scale with those of cryptic degassing, implying especially prolonged Siberian Traps cryptic degassing could explain early Triassic climate. We also note the FOAM palaeoclimate models embedded in SCION display low climate sensitivity, where a doubling of CO_2 leads to only ~3 °C of warming, compared with estimates of 3.5–5.5 °C/doubling of CO_2 from palaeoclimate observations and other models, which may lead to underestimation of the magnitude of warming[47].

Overall, the additional CO_2 emissions required to explain protracted warming are surprisingly subtle. Model scenarios incorporating an additional ~10^{12} mol CO_2 yr^{-1} from cryptic degassing for the duration of warming provide a much better match to climate records from the MMCO, EECO and Palaeocene than scenarios where the tempo of carbon release is solely defined by the tempo of volcanism. Sustaining the early Triassic hothouse requires an order of magnitude more cryptic degassing, ~10^{13} mol CO_2 yr^{-1} (Fig. 3c). Such fluxes represent only ~10% and ~100% increases, respectively, compared with estimated modern global volcanic carbon emissions[48].

Reconciling magmatic degassing and climate on 10^6–10^7 year timescales

Cryptic degassing from the lower crustal and mantle roots of LIP magma plumbing systems decoupled from surface volcanism, as proposed here, can explain multiple enigmatic features of Phanerozoic climate records. Climate–biogeochemical modelling underscores that volcanism alone is insufficient to drive observed carbon cycle disruptions. Evolving crustal rheology that decouples CO_2 flux from eruption rates can explain: (1) the relationship between geodynamically predicted 5–10-million-year timescales of mantle melting and observed <1 Myr main phase durations of volcanism in continental LIPs and (2) dual timescales of climate disruption including rapid pulses of warming and broad, long-term greenhouse intervals that lag the main phase of many LIPs. Development of more detailed climate records spanning intervals such as the Triassic–Jurassic and Pliensbachian–Toarcian could distinguish whether delayed recovery after climate-disrupting LIPs occurs selectively or is a ubiquitous feature of such events.

Through LIP life cycles we expect the highest proportions of cryptic degassing during two intervals: the 100s of kyr before and 1–10 Myr after the main phase of volcanism (Fig. 3d). Before the main phase of volcanism, the crust is cold and relatively low density, leading a higher proportion of magmas to solidify and exsolve volatiles in the middle to lower crust, according to prior modelling[4]. During the main phase, we expect high magma supply to inhibit crystallization-driven exsolution at depth, though ascending magmas and intrusions emplaced in the upper crust may still degas. Finally, we argue that this main phase then leads to a rheological transition in the crust, which curtails surface eruptions despite ongoing melt generation at depth. This leads to a waning interval dominated by cryptic degassing that can span the duration of mantle melting (1–10 Myr). In all cases, broad warming intervals that we attribute to cryptic degassing seem to lag the main phase of volcanism by 1–2 Myr, consistent with cooling timescales for 5–10-km thick melt-rich bodies at Moho depths (Methods). Further work is needed to understand the evolving transcrustal transport of magma and fluids through the LIP life cycle[3], which will refine the relationship between mantle melting, cryptic outgassing and observed climate. More broadly, the time evolution of cryptic degassing and thus climate recovery following the LIP main phase is likely to depend on inherited and time-evolving crustal properties, mantle melting history and tectonic forcing, pointing to a suite of factors influencing recovery trajectories observed after Phanerozoic LIPs. For example, future investigation could probe the role of rifting in sustaining particularly protracted Eocene warming after NAIP. Dynamics of recovery also depend on weathering of LIP basalt, which is expected to vary substantially across LIPs based on emplacement area and geographic position. This factor has a second-order impact in our climate–biogeochemical model for the Siberian Traps, Deccan, NAIP and CRB (Supplementary Fig. 4), but provisional model runs for the more poorly time-constrained Ethiopian LIP show that basalt weathering may balance total degassing in this case (Supplementary Fig. 3), muting the overall climate signal. For oceanic LIPs, which in some cases show geochronologic evidence for longer durations of volcanism[49], the potential for decoupling of surface volcanism from magma supply and cryptic degassing remains to be evaluated.

The tempo and pattern of climate recovery following mass extinction events may influence subsequent biological evolution as profoundly as the extinctions themselves[9,50–52]. For example, it has been suggested that elevated erosion and sediment flushing in the early Triassic—which we attribute to cryptic degassing-driven greenhouse conditions—enhanced microbial productivity in the oceans, delaying recovery of corals and filter feeders after the end-Permian mass extinction[52]. Suppressed mammalian diversification rates following the end-Cretaceous extinction also occur on the several Myr timescales predicted by cryptic degassing[53]. How cryptic solid Earth degassing combines with other factors including ecosystem dynamics and weathering to shape climate during recovery intervals thus illuminates the forces shaping diversification of life through Earth history.

Online content

Any methods, additional references, Nature Portfolio reporting summaries, source data, extended data, supplementary information, acknowledgements, peer review information; details of author contributions and competing interests; and statements of data and code availability are available at https://doi.org/10.1038/s41561-024-01574-3.

References

1. Courtillot, V. E. & Renne, P. R. On the ages of flood basalt events. *C. R. Geosci.* **335**, 113–140 (2003).
2. Clapham, M. E. & Renne, P. R. Flood basalts and mass extinctions. *Annu. Rev. Earth Planet. Sci.* **47**, 275–303 (2019).
3. Black, B. A., Karlstrom, L. & Mather, T. A. The life cycle of large igneous provinces. *Nat. Rev. Earth Environ.* **2**, 840–857 (2021).
4. Tian, X. & Buck, W. R. Intrusions induce global warming before continental flood basalt volcanism. *Nat. Geosci.* **15**, 417–422 (2022).
5. Gutjahr, M. et al. very large release of mostly volcanic carbon during the Palaeocene-eocene Thermal Maximum. *Nature* **548**, 573–577 (2017).

6. Black, B. A. et al. Systemic swings in end-Permian climate from Siberian Traps carbon and sulfur outgassing. *Nat. Geosci.* **11**, 949 (2018).
7. Cui, Y., Li, M., Van Soelen, E. E., Peterse, F. & Kürschner, W. M. Massive and rapid predominantly volcanic CO2 emission during the end-Permian mass extinction. *Proc. Natl Acad. Sci. USA* **118**, e2014701118 (2021).
8. Payne, J. L. & Kump, L. R. Evidence for recurrent Early Triassic massive volcanism from quantitative interpretation of carbon isotope fluctuations. *Earth Planet. Sci. Lett.* **256**, 264–277 (2007).
9. Payne, J. L. et al. Large perturbations of the carbon cycle during recovery from the end-Permian extinction. *Science* **305**, 506–509 (2004).
10. Joachimski, M. M. et al. Five million years of high atmospheric CO_2 in the aftermath of the Permian–Triassic mass extinction. *Geology* **50**, 650–654 (2022).
11. Burgess, S. D. & Bowring, S. A. High-precision geochronology confirms voluminous magmatism before, during, and after Earth's most severe extinction. *Sci. Adv.* **1**, e1500470 (2015).
12. Kasbohm, J. & Schoene, B. Rapid eruption of the Columbia River flood basalt and correlation with the mid-Miocene climate optimum. *Sci. Adv.* **4**, eaat8223 (2018).
13. Walker, J. C., Hays, P. B. & Kasting, J. F. A negative feedback mechanism for the long-term stabilization of Earth's surface temperature. *J. Geophys. Res.: Oceans* **86**, 9776–9782 (1981).
14. Babila, T. L. & Foster, G. L. in *Large Igneous Provinces: A Driver of Global Environmental and Biotic Changes* (eds Ernst, R. E. at al.) 401–416 (Wiley & Sons, 2021).
15. Kasbohm, J., Schoene, B. & Burgess, S. in *Large Igneous Provinces: A Driver of Global Environmental and Biotic Changes* (eds Ernst, R. E. et al.) 27–82 (Wiley & Sons, 2021).
16. Coffin, M. F. & Eldholm, O. Large igneous provinces: crustal structure, dimensions, and external consequences. *Rev. Geophys.* **32**, 1–36 (1994).
17. Ridley, V. A. & Richards, M. A. Deep crustal structure beneath large igneous provinces and the petrologic evolution of flood basalts. *Geochem. Geophys. Geosyst.* **11**, Q09006 (2010).
18. Glisovic, P. & Forte, A. M. On the deep-mantle origin of the Deccan Traps. *Science* **355**, 613–616 (2017).
19. Huber, C., Townsend, M., Degruyter, W. & Bachmann, O. Optimal depth of subvolcanic magma chamber growth controlled by volatiles and crust rheology. *Nat. Geosci.* **12**, 762–768 (2019).
20. Hunt, J. A., Zafu, A., Mather, T. A., Pyle, D. M. & Barry, P. H. Spatially variable CO_2 degassing in the main Ethiopian rift: implications for magma storage, volatile transport, and rift-related emissions. *Geochem. Geophys. Geosyst.* **18**, 3714–3737 (2017).
21. Lee, H. et al. Massive and prolonged deep carbon emissions associated with continental rifting. *Nat. Geosci.* **9**, 145–149 (2016).
22. Westerhold, T. et al. An astronomically dated record of Earth's climate and its predictability over the last 66 million years. *Science* **369**, 1383–1387 (2020).
23. Rae, J. W. et al. Atmospheric CO_2 over the past 66 million years from marine archives. *Annu. Rev. Earth Planet. Sci.* **49**, 609–641 (2021).
24. Chen, J. et al. High-resolution SIMS oxygen isotope analysis on conodont apatite from South China and implications for the end-Permian mass extinction. *Palaeogeogr. Palaeoclimatol. Palaeoecol.* **448**, 36–48 (2015).
25. Sun, Y. et al. Lethally hot temperatures during the Early Triassic greenhouse. *Science* **338**, 366–370 (2012).
26. Cenozoic CO2 Proxy Integration Project (CenCO2PIP) Consortium et al. Toward a Cenozoic history of atmospheric CO_2. *Science* **382**, eadi5177 (2023).
27. Callegaro, S. et al. Recurring volcanic winters during the latest Cretaceous: sulfur and fluorine budgets of Deccan Traps lavas. *Sci. Adv.* **9**, eadg8284 (2023).
28. Svensen, H. et al. Siberian gas venting and the end-Permian environmental crisis. *Earth Planet. Sci. Lett.* **277**, 490–500 (2009).
29. Cao, C. et al. Persistent late Permian to Early Triassic warmth linked to enhanced reverse weathering. *Nat. Geosci.* **15**, 832–838 (2022).
30. Berner, R. A., Lasaga, A. C. & Garrels, R. M. The carbonate-silicate geochemical cycle and its effect on atmospheric carbon dioxide over the past 100 million years. *Am. J. Sci.* **283**, 641–683 (1983).
31. Kent, D. V. & Muttoni, G. Equatorial convergence of India and early Cenozoic climate trends. *Proc. Natl Acad. Sci. USA* **105**, 16065–16070 (2008).
32. Alt, J. C. & Teagle, D. A. The uptake of carbon during alteration of ocean crust. *Geochim. Cosmochim. Acta* **63**, 1527–1535 (1999).
33. Müller, R. D. et al. Evolution of Earth's tectonic carbon conveyor belt. *Nature* **605**, 629–639 (2022).
34. Hoareau, G. et al. Did high neo-Tethys subduction rates contribute to early Cenozoic warming? *Climate* **11**, 1751–1767 (2015).
35. Jurikova, H. et al. Permian–Triassic mass extinction pulses driven by major marine carbon cycle perturbations. *Nat. Geosci.* **13**, 745–750 (2020).
36. McKay, D. I. A., Tyrrell, T., Wilson, P. A. & Foster, G. L. Estimating the impact of the cryptic degassing of large igneous provinces: a mid-Miocene case-study. *Earth Planet. Sci. Lett.* **403**, 254–262 (2014).
37. Hernandez Nava, A. et al. Reconciling early Deccan Traps CO_2 outgassing and pre-KPB global climate. *Proc. Natl Acad. Sci. USA* **118**, e2007797118 (2021).
38. Isson, T. T. et al. Marine siliceous ecosystem decline led to sustained anomalous Early Triassic warmth. *Nat. Commun.* **13**, 3509 (2022).
39. Glisovic, P. & Forte, A. M. Two deep-mantle sources for Paleocene doming and volcanism in the North Atlantic. *Proc. Natl Acad. Sci. USA* **116**, 13227–13232 (2019).
40. Farnetani, C. G. & Richards, M. A. Numerical investigations of the mantle plume initiation model for flood basalt events. *J. Geophys. Res.: Solid Earth* **99**, 13813–13833 (1994).
41. Karlstrom, L. & Richards, M. On the evolution of large ultramafic magma chambers and timescales for flood basalt eruptions. *J. Geophys. Res.: Solid Earth* **116**, B08216 (2011).
42. Mather, T. A. & Schmidt, A. in *Large Igneous Provinces: A Driver of Global Environmental and Biotic Changes* (eds Ernst, R. E. et al.) 103–116 (Wiley & Sons, 2021).
43. Mittal, T. & Richards, M. A. Volatile degassing from magma chambers as a control on volcanic eruptions. *J. Geophys. Res.: Solid Earth* **124**, 7869–7901 (2019).
44. Watanabe, N. et al. Potentially exploitable supercritical geothermal resources in the ductile crust. *Nat. Geosci.* **10**, 140–144 (2017).
45. Gleeson, T. & Ingebritsen, S. (eds). *Crustal Permeability* (Wiley & Sons, 2016).
46. Connolly, J. & Podladchikov, Y. Y. Compaction-driven fluid flow in viscoelastic rock. *Geodin. Acta* **11**, 55–84 (1998).
47. Farnsworth, A. et al. Climate sensitivity on geological timescales controlled by nonlinear feedbacks and ocean circulation. *Geophys. Res. Lett.* **46**, 9880–9889 (2019).
48. Werner, C. et al. in *Deep Carbon Past to Present* (eds Orcutt, B. N., Daniel, I. & Dasgupta, R.) (Cambridge Univ. Press, 2019).
49. Jiang, Q., Jourdan, F., Olierook, H. K. & Merle, R. E. An appraisal of the ages of Phanerozoic large igneous provinces. *Earth Sci. Rev.* **237**, 104314 (2023).
50. Monarrez, P. M., Heim, N. A. & Payne, J. L. Mass extinctions alter extinction and origination dynamics with respect to body size. *Proc. R. Soc. B* **288**, 20211681 (2021).

51. Hull, P. Life in the aftermath of mass extinctions. *Curr. Biol.* **25**, R941–R952 (2015).
52. Chen, Z. & Benton, M. J. The timing and pattern of biotic recovery following the end-Permian mass extinction. *Nat. Geosci.* **5**, 375–383 (2012).
53. Grossnickle, D. M., Smith, S. M. & Wilson, G. P. Untangling the multiple ecological radiations of early mammals. *Trends Ecol. Evol.* **34**, 936–949 (2019).
54. Schoene, B. et al. U-Pb constraints on pulsed eruption of the Deccan Traps across the end-Cretaceous mass extinction. *Science* **363**, 862–866 (2019).
55. Storey, M., Duncan, R. A. & Tegner, C. Timing and duration of volcanism in the North Atlantic Igneous Province: implications for geodynamics and links to the Iceland hotspot. *Chem. Geol.* **241**, 264–281 (2007).
56. Sprain, C. J. et al. The eruptive tempo of Deccan volcanism in relation to the Cretaceous-Paleogene boundary. *Science* **363**, 866–870 (2019).

Methods

Reconstruction of volcanic and metamorphic CO_2 emissions histories

The total carbon outgassing flux C_{total} from LIPs is given by:

$$C_{total} = C_{co\text{-}eruptive} + C_{cryptic} \quad (1)$$

Where the co-eruptive outgassing flux $C_{co\text{-}eruptive}$ is a combination of CO_2 that exsolves from erupting magmas and CO_2 from intrusive magmas ($C_{intrusive,co\text{-}eruptive}$), defined by the intrusive-to-extrusive ratio, and from sedimentary rocks ($C_{metamorphic,co\text{-}eruptive}$) heated by those magmas that is released during eruptions (rather than during non-eruptive intervals):

$$C_{co\text{-}eruptive} = C_{volcanic} + C_{metamorphic,co\text{-}eruptive} + C_{intrusive,co\text{-}eruptive} \quad (2)$$

We define the cryptic CO_2 flux as the flux of CO_2 gas during surface quiescence (that is, decoupled from surface eruptions), which could in principle combine both CO_2 from intrusive magmas and CO_2 from metamorphism:

$$C_{cryptic} = C_{metamorphic,cryptic} + C_{intrusive,cryptic} \quad (3)$$

Here we focus primarily on CO_2 from intrusive magmas as more amenable to constraints from geodynamic modelling and mantle geochemistry.

To demonstrate the importance of this final term, $C_{cryptic}$, for understanding long-term surface climate evolution, we reconstructed CO_2 emissions histories that account for all other terms (Fig. 2). Specifically, we reconstructed (1) volcanic-only CO_2 emissions ($C_{volcanic}$) for each LIP, (2) volcanic plus intrusive emissions ($C_{volcanic} + C_{1:E}$) with an *I:E* ratio ranging from 1:1 to 10:1, roughly the range of *I:E* ratios for continental LIPs[16–18] and (3) volcanic CO_2 emissions plus a pulse of combined mantle and metamorphic carbon release ($C_{volcanic} + C_{metamorphic}$) as proposed for the Siberian Traps and NAIP[5,35]. All CO_2 reconstructions are given in Supplementary Table 1. For each of these scenarios, we consider uncertainties in initial magmatic CO_2. CO_2 and Ba partition similarly during mantle melting and crystallization, and therefore CO_2/Ba ratios have been applied in a range of tectonic settings to estimate initial magmatic CO_2 prior to degassing. Following the approach of ref. 37 for the Deccan Traps, we use Ba concentrations from the highest MgO tholeiitic lavas from each LIP (from Baffin Island picrites for NAIP[57]; from Gudchikhinsky picrites from the Siberian Traps[58]; from Steens lavas from the CRB[59]), which are assumed to be the least affected by crustal contamination or complex crystallization histories. We consider both depleted and more enriched CO_2/Ba ratios from plume-associated magmas (that is, CO_2/Ba = 48 or CO_2/Ba = 130) and Ba concentrations from MgO-rich magmas from each LIP to obtain lower and upper estimates for CO_2 concentrations[60–62]. These estimates of CO_2 concentrations are combined with volume estimates for each formation to yield reconstructed volcanic CO_2 release (Supplementary Fig. 2 and Supplementary Table 1). For the Siberian Traps, CRB and NAIP, we do not attempt to account for evolving CO_2 through the course of LIP emplacement because insufficient constraints are available to do so rigorously, though we acknowledge that mantle sources and melting conditions for individual formations are likely to have varied, resulting in variations in CO_2[63]. As an initial approximation, we assume such variations in initial CO_2 to be encapsulated within the range of parental CO_2 concentrations we consider.

Unlike the CRB and Deccan Traps, the formation-level tempo of lava emplacement in the Siberian Traps and NAIP is not well constrained. For the Siberian Traps, we therefore assume two phases of lava emplacement separated by an extrusive hiatus, following the chronology of ref. 64. For the NAIP, we similarly assume two phases of lava emplacement separated by a longer hiatus[55], though the existence of such a hiatus versus more continuous volcanic activity has recently been called into question[65]. Additional geochronologic data would further refine timelines of volcanic CO_2 release, in particular for the NAIP and the Siberian Traps.

For scenarios including metamorphic degassing, we draw on published estimates of 10,200–12,200 Pg C during the PETM and two-phase release of 96,000 Pg C during the end-Permian[5,35].

Palaeoclimate proxy records

Surface temperature variations since the latest Cretaceous (Fig. 1) are based on the CENOGRID compilation of marine oxygen isotope records. Surface temperatures are calculated from oxygen isotope records using the methodology of ref. 66. Cenozoic CO_2 data are drawn from compilations of seawater boron isotope records[23,26], which provide a proxy for marine pH, which in turn depends on atmospheric pCO_2.

Permian–Triassic equatorial surface temperature variations (Fig. 2d) are based on oxygen isotope measurements in conodonts from South China. The age model in ref. 25 has been adjusted to account for the updated U–Pb zircon age of bed 27d of 251.88 Ma, consistent with the age model in ref. 24. Supplementary Table 2 summarizes availability of palaeoclimate data and patterns of recovery for continental LIPs of the past 260 Myr.

Crustal sequestration

Determining the proportion of exsolved CO_2 sequestered in the crust through metamorphic reactions is an active area of research. Indeed, some evidence suggests that if carbonate-bearing crustal rocks are present, magmatic fluids permeating through the crust can drive decarbonation reactions, in which silica-saturated magmatic fluids react with crustal carbonates to yield calc-silicates and CO_2, potentially adding an additional metamorphic CO_2 flux to the magmatic CO_2 flux to the atmosphere[67]. In other words, it is possible reactive passage through the crust may increase rather than decrease CO_2 fluxes to the atmosphere. However, silica solubility decreases with increasing X_{CO2} in H_2O–CO_2 fluids[68], and therefore for the CO_2-rich fluids considered here, we expect this to be a secondary effect. Overall, major questions remain for the behaviour of volatiles as they pass through the crust. However, available evidence suggests it is reasonable to assume the majority of CO_2 reaches the atmosphere.

Mantle geodynamics modelling

We model plume ascent and melt generation using numerical geodynamic models closely following Leitch and Davies[69], who considered melt generation from a plume head that incorporates eclogite in addition to peridotite. The mantle is treated as an incompressible viscous medium. We solve the equations describing conservation of mass, momentum and energy under the Boussinesq approximation in cylindrical axisymmetric coordinates using conservative finite differences with a marker-in-cell approach[70]. The depth of the domain is 2,850 km and the domain extends 1,000 km from the axis of symmetry. The cell size is 7.5 km × 7.5 km and we use 288 markers per cell. We use a simplified representation of mantle viscosity that includes temperature and depth-dependence with the form

$$\eta_{mantle} = \eta(z)\exp\left(\frac{E}{RT_{ref}}\left(\frac{T_{ref}}{T} - 1\right)\right) \quad (4)$$

where E = 300 kJ mol^{-1} is the activation energy, R is the universal gas constant and T_{ref} = 1,300 °C is the reference temperature. The depth-dependence $\eta(z)$ assumes an upper mantle reference viscosity of 5×10^{19} Pa-s and a 20-fold viscosity increase at 660 km depth.

We assume a mantle of initial uniform temperature 1,300 °C following prior work[69]. The boundary layer from which the ascending plume is generated contains 15% eclogitic material[69,71] (uncertainty

envelopes in Supplementary Fig. 1b,d show effects of varying this proportion from 5 to 25%) and has a temperature structure described by half-space cooling with a characteristic thickness that varies linearly from 150 km along the axis of symmetry to 112 km at the boundary of the domain. The initial thermal structure of the lithosphere is prescribed using a half-space cooling model defined by a characteristic thickness of 60 or 90 km. We re-assimilate the thermal structure of the lithosphere when melting begins to enforce the desired thickness during LIP melting[69].

Melting is computed for eclogite using laboratory-derived melt curves[72], assuming that melt fraction varies linearly between the solidus and liquidus[69] and adopting an upper mantle adiabat of 0.4 °C km^{-1}. We compute and track melting on the Lagrangian markers/particles. The total rate of melt generation is computed by numerical integration, accounting for the axisymmetric geometry. In calculations of CO_2 release, CO_2 is assumed to be perfectly incompatible during melting and we therefore assume that when a parcel of mixed peridotite and eclogite undergoes melting, CO_2 is completely extracted from both lithologies. Following prior work, eclogitic mantle is assumed to contain 900–1,800 ppm CO_2 (ref. 71). Peridotitic upper mantle is assumed to contain 137–400 ppm CO_2, based on measurements of undegassed mid-ocean ridge melt inclusion suites[73] and CO_2/Ba ratios combined with Ba concentrations in the convecting mantle[74]. These ranges in mantle source CO_2 are used to define a first-order uncertainty envelope for cryptic degassing (Supplementary Fig. 1).

Transcrustal magma transport modelling

LIPs represent an end-member of volcanism on Earth, producing enormous eruptive episodes with no historic analogue. As in other settings, crustal rheology probably exerts primary control on the depth and stability of crustal magma reservoirs. With progressive heating, the mechanical response of crustal rocks becomes increasingly ductile, eventually inhibiting the build-up of deviatoric stresses needed to drive dike formation. We model the impact of magmatic heat on crustal rheology to determine the transition point to dominantly ductile response; we consider this to indicate a transition to intrusion-dominated magmatism and decoupling of surface eruptions from continued mantle melting. LIP eruptions require massive storage zones, although whether these storage zones form single large 'tanks'[75] or a distribution of smaller, syn-eruptively mobilized intrusions[76], remains a matter of debate. Cooling and crystallization of a single large intrusion cannot explain the protracted multi-million-year duration of cryptic degassing required to match palaeoclimate records: cooling time is roughly equivalent to a conduction timescale based on intrusion thickness (~ 0.8–3 Myr for thickness of 5–10 km and diffusivity of 10^{-6} m^2 s^{-1}) even when multicomponent melt fraction–temperature parameterizations are accounted for. This cooling timescale provides one plausible mechanism to explain the apparent lag between abrupt co-eruptive warming and the broad, long-term warming we attribute to cryptic degassing, underscoring this as an avenue for future investigation with more sophisticated models that couple mantle melting, magma chamber dynamics and degassing.

We solve a transient 1D conduction equation, modelling magma transport as a slowly evolving volumetric heat source spread uniformly over a region spanning the mid to lower crust height L. We solve

$$\rho c_\mathrm{p}\frac{\partial T}{\partial t} = k\frac{\partial^2 T}{\partial z^2} + H(z,t), \tag{5}$$

subject to prescribed surface temperature and mantle heat flow, where ρ, c_p and k are bulk density, specific heat capacity and thermal conductivity of the crustal volume. Flux of mantle melts into the volume $Q(t)$ is assumed to comprise of a stochastic distribution of intrusions that release sensible and latent heat according to

$$H(z,t) = \frac{Q(t)}{2V}\left(1+\tanh\left[10\frac{z-L}{H}\right]\right)\rho\epsilon\left(c_\mathrm{p}\Delta T + L_\mathrm{f}\right) \tag{6}$$

With $V = \pi R^2 L$ the assumed volume where quasi-continuous intrusions occur (radius R and height L), ΔT is the average temperature difference between liquidus magma and crust and L_f is the latent heat of fusion. ϵ is a magmatic heating efficiency factor to account for unmodelled mechanical energy dissipation and heat transport within the volume. We take $\epsilon = 0.01$ based on spatially resolved simulations of stochastic lower crustal intrusions[77], which demonstrate low overall conversion of thermal energy to melting during distributed intrusion episodes.

We model temperature dependent crustal rheology through an Arrhenius law $\eta_\mathrm{crust} = A\exp(\frac{B}{T})$ with A and B a scaling constant (includes activation energy and gas constant, taken from ref. 78), which defines a Maxwell relaxation time $\tau_\mathrm{relax} = \eta_\mathrm{crust}/G$, with $G = 10$ GPa an effective elastic modulus of the crust. A rheologic transition to ductile dominated deformation[79] is assumed to occur when $\frac{\tau_\mathrm{relax}}{\tau_\mathrm{strain}} = 1-10$, where $\tau_\mathrm{strain} = \frac{V_\mathrm{ch}}{Q}$ is the characteristic recharge timescale for individual intrusions with volume $V_\mathrm{ch} = 500\,\mathrm{km}^3$. To make the regime diagram in Fig. 3b, we run a grid of transient heating simulations that solve equation (4) with finite differences[80] spanning a range of intruded volume heights L and (constant) mantle influx rates Q, ending the simulations when $\frac{\tau_\mathrm{relax}}{\tau_\mathrm{strain}} = 1$ at the shallowest point in V. This timescale is coloured in Fig. 3b. In reality, the parameter space for this problem is much larger than L and Q—in general one would need both to refine the thermomechanical model for heat and mass transfer and the rheological model of crustal rocks. However, deviatoric stress amplitude decreases as a doubly exponential function of time[41]. This makes the order of magnitude timescales of rheological weakening fairly robust to parameter choices.

Climate–biogeochemical modelling

To capture the climate and carbon cycle response to LIP CO_2 release, we use the SCION (Spatial Continuous IntegratiON) model[81]. SCION combines Earth's long-term carbon, oxygen, sulfur and nutrient cycles with a 3D steady state climate module to evaluate the processes that control climate and Earth surface chemistry over deep time. Because it has a spatially resolved climate and continental surface, it can simulate both the CO_2 degassing from LIPs and the CO_2 removal through silicate weathering over millions of years. In addition to the silicate weathering feedback, SCION also responds to warming by increasing the global weathering-derived delivery of terrestrial and marine nutrients, ultimately resulting in burial of organic carbon and further drawdown of CO_2. Extensive documentation for the model, and the code, is freely available at https://github.com/bjwmills/SCION. The model has been tested over the Phanerozoic and produces a reasonable fit to the broad evolution of CO_2, $\delta^{13}C_\mathrm{carbonate}$ and $\delta^{34}S_\mathrm{sulfate}$ proxy data over this time, where δ indicates per mil changes in carbon and sulfur isotope ratios relative to the Pee Dee Belemnite and Vienna-Canyon Diablo Troilite standards, respectively. SCION has previously been applied to the CRB degassing and weathering, where it showed that replicating the magnitude of global warming would require an additional degassing flux[82].

To quantify the possible cooling effect of these LIPs on global climate through additional silicate weathering, we altered the SCION model to incorporate the contribution of LIP rocks to the silicate weathering cycle[83]. We used a published LIP database[84], which provides a series of polygons representing estimated LIP extent at time of eruption and an exponential decay equation, to describe how LIP area changes through time. We reconstructed the LIP polygons using *pyGPlates* to each time grid of the SCION model and then rasterized them onto a 40 by 48 grid cell, such that they form a second palaeogeographic layer of the same dimensions as the default palaeogeographic maps. Some manual manipulation of these reconstructed grid cells was required. In these LIP maps, each cell was initially (that is, at LIP emplacement time) assigned a '1' if it was within a LIP footprint and a '0' otherwise. To account for the gradual erosion of LIPs through time, we use the

reconstructed LIP age (that is LIP emplacement time − SCION time grid) to calculate the area decay using equations (7) and (8). The result of these equations is a fractional number (0–1) representing the remaining LIP area present in each cell based on their age. This number is used to update the LIP-map values, such that each cell records the areal content of LIP material remaining based on its age. We use the following equations from ref. 84:

$$A_{\mathrm{decay}} = A\, e^{-\lambda t} \tag{7}$$

$$\lambda = \frac{\log(2)}{T_{1/2}} \tag{8}$$

With A being the original LIP area at time of emplacement; λ, the decay constant calculated in equation (6); t, time since emplacement (that is, the age of the LIP at analysis time) and $T_{1/2}$, the calculated half-life (= 29 Ma) from ref. 84.

The model considers all land other than LIPs to be a silicate mixture, which is seven times less weatherable than LIP material, a value which reflects the roughly sevenfold more weatherable nature of mafic LIP rock compared with typical continental crust[85]. As such, the fractional LIP coverage value is multiplied by 7 to yield a value for weathering from each grid square. This is in line with previous work investigating LIP weathering via the SCION model[82].

For most LIPs, weathering leads to modest cooling relative to the null case; this cooling is typically exceeded by warming due to CO_2 release. In the case of the Ethiopian Traps, excess CO_2 emissions and excess weathering of flood basalts nearly balance (Supplementary Fig. 3), leaving a minimal climate signal.

A key uncertainty in the model comparisons to data in this paper is SCION's relatively low climate sensitivity, which is inherited from the FOAM (Fast Ocean Atmosphere Model) climate model used to produce the steady state climate datasets[86]. More modern GCMs typically have higher climate sensitivity[87] and thus the SCION model might produce more warming for a given CO_2 input if updated with climate fields from these models. However, this would not by itself (that is, in the absence of factors such as cryptic degassing) cause the model to adequately match the surface temperature datasets in Fig. 2, which show temperature to be increasing or stable over long periods where simulations with only co-eruptive degassing predict temperature would be decreasing.

SCION predictions are compared with records of $\delta^{13}C_{carbonate}$ in Supplementary Fig. 5. This comparison is limited by uncertainties in the $\delta^{13}C$ of magmatic outgassing and weathering fluxes[88,89] and the array of factors influencing carbon burial and the composition of that carbon. It is therefore not surprising that SCION predictions display substantial misfits with carbon isotope records. For example, the early Triassic hosts multiple global swings in $\delta^{13}C$, which are not reproduced in the model[9]. Specifically, mismatches in the structure of marine carbon isotope records during recovery may result from a combination of fluctuating carbon burial or $\delta^{13}C$ of weathered or buried carbon[9], release of isotopically light carbon from metamorphism[8,28] or changing photosynthetic fractionation factors, making such mismatches difficult to interpret. Changes in carbon burial—possibly driven by fluctuations in marine productivity and oxygenation—have been proposed following the end-Permian[9], the end-Cretaceous[90], the PETM[5] and the MMCO[82]. The model $\delta^{13}C_{carbonate}$ predictions are generally closer to the geological record when cryptic degassing is considered, compared to when it is not, due to elevated input rates of isotopically light carbon, suggesting that overall cryptic degassing (among a suite of other factors influencing marine $\delta^{13}C$) is consistent with carbon isotope records.

Data availability

Palaeoclimate data are freely available from the references cited within the text and are also available via Zenodo at https://doi.org/10.5281/zenodo.13713036 (ref. 91), alongside CO_2 and melt generation envelopes, co-eruptive CO_2 reconstructions and SCION outputs. CO_2 emissions histories are also provided in Supplementary Table 1.

Code availability

The ASPECT geodynamic model can be downloaded at https://aspect.geodynamics.org. The SCION model is freely available at https://github.com/bjwmills/SCION. The one-dimensional diffusion model used to model magmatically induced crustal rheological shifts is freely available at https://github.com/leifkarlstrom/reverse_energy_cascade.

References

57. Kent, A. et al. Mantle heterogeneity during the formation of the North Atlantic igneous province: constraints from trace element and Sr–Nd–Os–O isotope systematics of Baffin Island picrites. *Geochem. Geophys. Geosyst.* **5**, Q11004 (2004).
58. Sobolev, A. V., Krivolutskaya, N. A. & Kuzmin, D. V. Petrology of the parental melts and mantle sources of Siberian trap magmatism. *Petrology* **17**, 253–286 (2009).
59. Moore, N. E., Grunder, A. L. & Bohrson, W. A. The three-stage petrochemical evolution of the Steens Basalt (southeast Oregon, USA) compared to large igneous provinces and layered mafic intrusions. *Geosphere* **14**, 2505–2532 (2018).
60. Hauri, E. H. et al. CO_2 content beneath northern Iceland and the variability of mantle carbon. *Geology* **46**, 55–58 (2018).
61. Rosenthal, A., Hauri, E. H. & Hirschmann, M. M. Experimental determination of C, F, and H partitioning between mantle minerals and carbonated basalt, CO_2/Ba and CO_2/Nb systematics of partial melting, and the CO_2 contents of basaltic source regions. *Earth Planet. Sci. Lett.* **412**, 77–87 (2015).
62. Matthews, S., Shorttle, O., Rudge, J. F. & Maclennan, J. Constraining mantle carbon: CO_2-trace element systematics in basalts and the roles of magma mixing and degassing. *Earth Planet. Sci. Lett.* **480**, 1–14 (2017).
63. Black, B. A. & Gibson, S. A. Deep carbon and the life cycle of large igneous provinces. *Elements* **15**, 319–324 (2019).
64. Burgess, S. D., Muirhead, J. D. & Bowring, S. A. Initial pulse of Siberian Traps sills as the trigger of the end-Permian mass extinction. *Nat. Commun.* **8**, 164 (2017).
65. Wilkinson, C. M., Ganerød, M., Hendriks, B. W. & Eide, E. A. Compilation and appraisal of geochronological data from the North Atlantic Igneous Province (NAIP). *Geol. Soc. London Special Publ.* **447**, 69–103 (2017).
66. Hansen, J., Sato, M., Russell, G. & Kharecha, P. Climate sensitivity, sea level and atmospheric carbon dioxide. *Philos. Trans. R. Soc. A* **371**, 20120294 (2013).
67. Chu, X., Lee, C. A., Dasgupta, R. & Cao, W. The contribution to exogenic CO_2 by contact metamorphism at continental arcs: a coupled model of fluid flux and metamorphic decarbonation. *Am. J. Sci.* **8**, 631–657 (2019).
68. Newton, R. C. & Manning, C. E. Hydration state and activity of aqueous silica in H_2O-CO_2 fluids at high pressure and temperature. *Am. Mineral.* **94**, 1287–1290 (2009).
69. Leitch, A. M. & Davies, G. F. Mantle plumes and flood basalts: enhanced melting from plume ascent and an eclogite component. *J. Geophys. Res.: Solid Earth* **106**, 2047–2059 (2001).
70. Gerya, T. V. & Yuen, D. A. Characteristics-based marker-in-cell method with conservative finite-differences schemes for modeling geological flows with strongly variable transport properties. *Phys. Earth Planet. Inter.* **140**, 293–318 (2003).
71. Sobolev, S. V. et al. Linking mantle plumes, large igneous provinces and environmental catastrophes. *Nature* **477**, 312–U80 (2011).
72. Yasuda, A., Fujii, T. & Kurita, K. Melting phase relations of an anhydrous mid-ocean ridge basalt from 3 to 20 GPa: implications for the behavior of subducted oceanic crust in the mantle. *J. Geophys. Res.: Solid Earth* **99**, 9401–9414 (1994).

73. Le Voyer, M., Kelley, K. A., Cottrell, E. & Hauri, E. H. Heterogeneity in mantle carbon content from CO_2-undersaturated basalts. *Nat. Commun.* **8**, 14062 (2017).
74. Hirschmann, M. M. Comparative deep Earth volatile cycles: the case for C recycling from exosphere/mantle fractionation of major (H_2O, C, N) volatiles and from H_2O/Ce, CO_2/Ba, and CO_2/Nb exosphere ratios. *Earth Planet. Sci. Lett.* **502**, 262–273 (2018).
75. Annen, C., Latypov, R., Chistyakova, S., Cruden, A. R. & Nielsen, T. F. Catastrophic growth of totally molten magma chambers in months to years. *Sci. Adv.* **8**, eabq0394 (2022).
76. Mittal, T. & Richards, M. A. The magmatic architecture of continental flood basalts: 2. a new conceptual model. *J. Geophys. Res.: Solid Earth* **126**, e2021JB021807 (2021).
77. Dufek, J. & Bergantz, G. W. Lower crustal magma genesis and preservation: a stochastic framework for the evaluation of basalt–crust interaction. *J. Petrol.* **46**, 2167–2195 (2005).
78. Jellinek, A. M. & DePaolo, D. J. A model for the origin of large silicic magma chambers: precursors of caldera-forming eruptions. *Bull. Volcanol.* **65**, 363–381 (2003).
79. Rucker, C., Erickson, B. A., Karlstrom, L., Lee, B. & Gopalakrishnan, J. A computational framework for time-dependent deformation in viscoelastic magmatic systems. *J. Geophys. Res.: Solid Earth* **127**, e2022JB024506 (2022).
80. Karlstrom, L., Paterson, S. R. & Jellinek, A. M. A reverse energy cascade for crustal magma transport. *Nat. Geosci.* **10**, 604–608 (2017).
81. Mills, B. J., Donnadieu, Y. & Godderis, Y. Spatial continuous integration of Phanerozoic global biogeochemistry and climate. *Gondwana Res.* **100**, 73–86 (2021).
82. Longman, J., Mills, B. J., Donnadieu, Y. & Goddéris, Y. Assessing volcanic controls on Miocene climate change. *Geophys. Res. Lett.* **49**, e2021GL096519 (2022).
83. Longman, J., Mills, B. & Merdith, A. Limited long-term cooling effects of flood basalt emplacements. Preprint at https://doi.org/10.31223/X5HQ3F (2024).
84. Park, Y., Swanson-Hysell, N. L., Lisiecki, L. E. & Macdonald, F. A. in *Large Igneous Provinces: A Driver of Global Environmental and Biotic Changes* (eds Erns, R. E. et al.) 153–168 (2021).
85. Dessert, C., Dupré, B., Gaillardet, J., François, L. M. & Allegre, C. J. Basalt weathering laws and the impact of basalt weathering on the global carbon cycle. *Chem. Geol.* **202**, 257–273 (2003).
86. Donnadieu, Y. et al. A GEOCLIM simulation of climatic and biogeochemical consequences of Pangea breakup. *Geochem. Geophys. Geosyst.* **7**, Q11019 (2006).
87. Tierney, J. E. et al. Past climates inform our future. *Science* **370**, eaay3701 (2020).
88. Bachan, A. & Payne, J. L. Modelling the impact of pulsed CAMP volcanism on pCO_2 and $\delta^{13}C$ across the Triassic–Jurassic transition. *Geol. Mag.* **153**, 252–270 (2016).
89. Gales, E., Black, B. & Elkins-Tanton, L. T. Carbonatites as a record of the carbon isotope composition of large igneous province outgassing. *Earth Planet. Sci. Lett.* **535**, 116076 (2020).
90. Cox, A. A. & Keller, C. B. A Bayesian inversion for emissions and export productivity across the end-Cretaceous boundary. *Science* **381**, 1446–1451 (2023).
91. Black, B. A., Karlstrom, L., Mills, B. J. W., Mather, T. A., Rudolph, M. L., Longman, J. & Merdith, A. Data repository: cryptic degassing and protracted greenhouse climates after flood basalt events. *Zenodo* https://doi.org/10.5281/zenodo.13713036 (2024).

Acknowledgements

We acknowledge support from NSF 2317935 (B.A.B.) and the Alfred P. Sloan Foundation (B.A.B.), NSF 1848554 and 2317936 (L.K.), NSF 2317937 (M.L.R.), the UK Natural Environment Research Council (NERC) grants NE/Y00650X/1 (B.J.W.M. and T.A.M.), NE/X011208/1 (B.J.W.M. and A.M.), and NE/S009663/1 (B.J.W.M.) and Australian Research Council DECRA Fellowship DE230101642 (A.M.).

Author contributions

B.A.B., L.K. and T.A.M. conceived the project. B.A.B. compiled proxy and volcanic CO_2 data. L.K., B.J.W.M., B.A.B., and M.L.R. ran the models with input from J.L. and A.M. All authors contributed to writing the manuscript.

Competing interests

The authors declare no competing interests.

Additional information

Supplementary information The online version contains supplementary material available at https://doi.org/10.1038/s41561-024-01574-3.

Correspondence and requests for materials should be addressed to Benjamin A. Black.

Peer review information *Nature Geoscience* thanks Matthew Clapham, Sarah Greene and the other, anonymous, reviewer(s) for their contribution to the peer review of this work. Primary Handling Editor: James Super, in collaboration with the *Nature Geoscience* team.